Journal of Applied Electrochemistry **31**: 349–354, 2001.

Tin–cobalt electrodeposition from sulfate–gluconate baths

E. GÓMEZ[1], E. GUAUS[2], J. TORRENT[2], X. ALCOBE[3] and E. VALLÉS[1]*
[1]*LCTEM, Departament de Química Física, Universitat de Barcelona, Martí i Franques, 1, 08028 Barcelona, Spain*
[2]*Departament d'Enginyeria Química, Universitat Politècnica de Catalunya, Colom, 1, 08222 Terrassa, Spain*
[3]*Serveis Cientificotècnics, Universitat de Barcelona, Lluis Solé i Sabaris, 1–3, 08028 Barcelona, Spain*
*(*author for correspondence, e-mail: e.valles@qf.ub.es)*

Received 4 May 2000; accepted in revised form 2 October 2000

Key words: alloys, electrodeposition, stripping, tin–cobalt, XRD

Abstract

The electrodeposition of tin + cobalt alloys from a slightly acidic sulfate–gluconate bath on both vitreous carbon and copper substrates has been studied for different [Sn(II)]/[Co(II)] ratios in the bath, varying between 1/10 and 1/2. A relationship between the electrochemical stripping analysis and the morphology of the deposits has been found. Two different types of deposit were obtained. At low [Sn(II)]/[Co(II)] ratios and relatively high deposition rates a nodular, cobalt-rich, nanocrystalline coating was obtained, while at high [Sn(II)]/[Co(II)] ratios and low deposition rates a new, well-defined tetragonal SnCo phase was obtained, with cell parameters of $a = 3.087$ Å and $c = 5.849$ Å. This structure favours hydrogen evolution.

1. Introduction

Although the electrodeposition of tin–cobalt alloys was first described in 1938, only recently has it achieved commercial interest as a noncontaminating, economic way to an attractive and functional finish [1]. Bright tin–cobalt coatings are considered to be a substitute for chromium coatings, especially where the high corrosion resistance of chromium is not needed [2, 3]. Tin–cobalt alloy plating could also be a substitute for cadmium in electronic applications [4], since the alloy resists oxidation and has a low contact resistance. Tin–cobalt alloys can be used as a substitute of precious-metal coatings [5], thereby avoiding the use of highly toxic cyanide electrolytes. Electrodeposited black tin–cobalt alloy has also been used for plating photothermal solar convectors [6, 7].

One of the baths for tin–cobalt alloy plating uses sodium sulfate as electrolyte and sodium gluconate as chelating agent. Various authors [1, 3, 8] have studied the effect of some operating variables on the physical and mechanical properties of the Sn/Co deposits obtained in this bath under galvanostatic control. Abd el Rehim et al. [8] reported the potentiodynamic behaviour of the system and studied the relation between structure and composition of electrodeposits. Other authors [9] used Mössbauer spectroscopy to examine the composition and structure of electrodeposited tin–cobalt alloys plated under galvanostatic control, and concluded that the relative amounts of Sn and Co were dependent on the operating conditions.

In this study the electrodeposition of tin–cobalt coatings was performed in a slightly acidic sulfate bath using gluconate as a chelating agent, in order to determine the dependence of coating characteristics on several electroplating variables. Potentiodynamic studies and stripping experiments were used to characterize the deposits, since the stripping technique has been shown to be useful for the characterization of other electrodeposited alloys [10–13]. These results were related to those obtained from morphological and structural analysis and to compositional data.

2. Experimental details

The electrochemical measurements were performed in a conventional three-electrode cell using a microcomputer-controlled potentiostat/galvanostat, model 273 from EG&G. Chemicals used were $SnSO_4$, $CoSO_4 \cdot 7\ H_2O$, sodium gluconate ($NaC_6H_{11}O_7$) and Na_2SO_4, all of them of analytical grade. All solutions were freshly prepared with water first doubly distilled and then fed into a Millipore Milli Q system. In all experiments the total metallic ion concentration was maintained around 0.1 M, the [Sn(II)]/[Co(II)] ratio varying between 1/10 and 1/2. The baths contained Na_2SO_4 0.2 M as supporting electrolyte and $NaC_6H_{11}O_7$ 0.2 M as chelating agent, and the pH was adjusted to 4. Before and during the experiments, solutions were deaerated with argon.

The morphology of the deposits was examined with a Hitachi S 2300 scanning electron microscope. Elemental

composition was determined with an X-ray analyser incorporated in a Cambridge L-120 scanning electron microscope, or with an electron microprobe, Cameca SX-50. X-ray diffraction (XRD) phase analysis was usually performed in a Philips MRD diffractometer in its low resolution parallel beam optics. The CuK_α radiation ($\lambda = 1.5418$ Å) was selected by means of a diffracted beam flat graphite monochromator. $2\theta/\theta$ diffractograms were obtained in the 20 to 100° 2θ ranges with a step of 0.05° and a measuring time of 5″ per step. For the profile pattern matching analysis, additional X-ray diffraction measurements were performed. A Bragg–Brentano $\theta/2\theta$ Siemens D-500 diffractometer with CuK_α radiation, secondary graphite beam, 0.3° divergence slit and 0.05° receiving slit, was used. The useful angular range was from 27 to 81° 2θ, measured with an step size of 0.025° and a measuring time of 10″.

Vitreous carbon and copper were used as working electrodes. The vitreous carbon electrode of 0.0314 cm^2, from Metrohm, was polished to a mirror finish before each experiment using alumina of different grades (3.75 and 1.85 μm) and cleaned ultrasonically for 2 min in water. Copper electrodes either of 0.0314 or 0.706 cm^2 (Johnson Matthey, 99.99%) were polished to a mirror finish using a 0.3 μm alumina suspension and cleaned ultrasonically for 2 min in water. The reference electrode was an Ag/AgCl/1 M NaCl electrode mounted in a Luggin capillary containing 0.2 M Na_2SO_4 solution. All potentials are referred to this electrode. The counter electrode was a platinum spiral. Voltammetric experiments were carried out at 50 mV s^{-1}, scanning initially towards negative potentials. Only one cycle was run in each voltammetric experiment. Stripping analyses were always performed immediately after potentiostatic deposition without removing the electrode from the solution, using an initial potential at which deposition did not occur and a scan rate of 50 mV s^{-1}.

3. Results

3.1. *Voltammetric results*

Figure 1 shows the influence of Sn(II) addition to Co(II) solution. Curve (a) shows the voltammetric behaviour of the electrodeposition of cobalt in a pure Co(II) bath. When Sn(II) was added to solution (curve (b), dashed line), in the negative scan the deposition of tin precedes the second electrodeposition process related to the incorporation of cobalt in the electrodeposit. In the positive scan, oxidation was detected in the potential range at which the oxidation of pure tin takes place, although the current recorded was lower than that observed in a cobalt-free solution (curve (c)). The main oxidation peak is shifted to more positive potentials than in a pure Co(II) bath. Therefore, in these conditions, the deposit (Sn + Co alloy) formed during the voltammetric scan was more difficult to oxidize than the corresponding to pure cobalt.

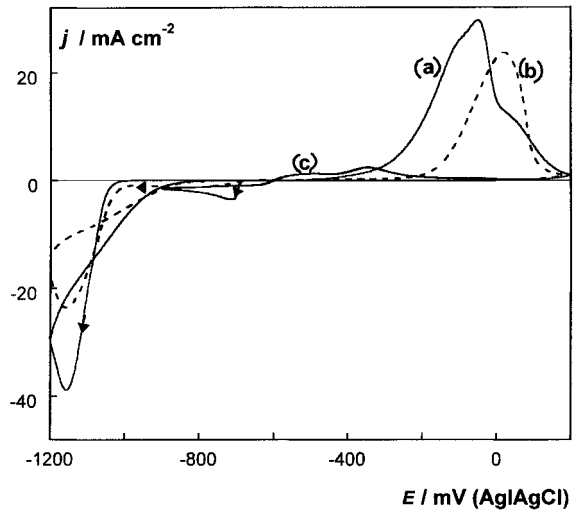

Fig. 1. Cyclic voltammograms of a vitreous carbon electrode in 0.1 M $CoSO_4$ + 0.2 M $NaC_6H_{11}O_7$ + 0.2 M Na_2SO_4 solution (curve (a)), 0.1 M $CoSO_4$ + 0.01 M $SnSO_4$ + 0.2 M $NaC_6H_{11}O_7$ + 0.2 M Na_2SO_4 solution (dashed line, curve (b)) and 0.01 M $SnSO_4$ + 0.2 M $NaC_6H_{11}O_7$ + 0.2 M Na_2SO_4 solution (curve (c)).

Upon increasing the [Sn(II)]/[Co(II)] ratio in the bath the oxidation current decreased drastically, so much so that for [Sn(II)]/[Co(II)] = 1/2 the main oxidation peak disappeared, only a low tin oxidation current being observed (Figure 2).

3.2. *Stripping results*

Stripping analysis of all the potentiostatic deposits was performed. The deposition potentials were selected according to previous voltammetric results, and the solution was stirred during the electrodeposition in order to minimize the depletion of ions around the electrode.

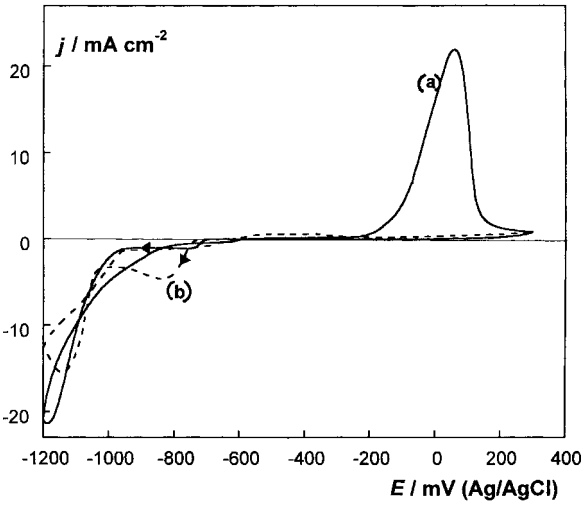

Fig. 2. Cyclic voltammograms of a vitreous carbon electrode in a 0.1 M $CoSO_4$ + 0.01 M $SnSO_4$ + 0.2 M $NaC_6H_{11}O_7$ + 0.2 M Na_2SO_4 solution (solid line, curve (a)) and 0.06 M $CoSO_4$ + 0.03 M $SnSO_4$ + 0.2 M $NaC_6H_{11}O_7$ + 0.2 M Na_2SO_4 solution (dashed line, curve (b)).

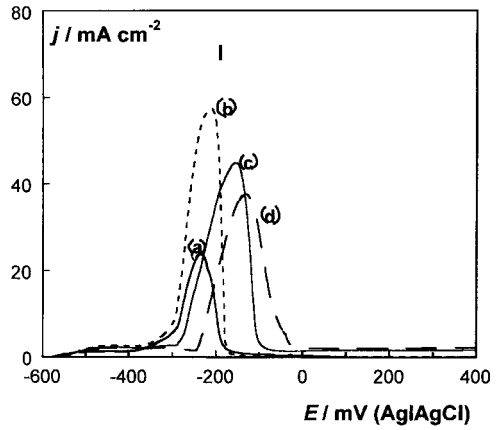

Fig. 3. Stripping voltammograms of deposits obtained potentiostatically on a vitreous carbon electrode rotating at 1000 rpm in a 0.01 M $SnSO_4$ + 0.2 M $NaC_6H_{11}O_7$ + 0.2 M Na_2SO_4 solution for 20 s at −850 mV (curve (a)) and in a 0.06 M $CoSO_4$ + 0.03 M $SnSO_4$ + 0.2 M $NaC_6H_{11}O_7$ + 0.2 M Na_2SO_4 solution at −920 mV for 10 s (curve (b)), at −960 mV for 10 s (curve (c)) and at −1000 mV for 10 s (curve (d)).

Figure 3 shows the stripping curves corresponding to deposits obtained at potentials more positive than −1000 mV, from a pure Sn bath (curve (a)) and from a [Sn(II)]/[Co(II)] = 1/2 bath (curves (b)–(d)). All stripping curves show a single peak (peak I) over a limited potential range for both pure Sn and Sn + Co alloys, no new peaks appearing when the deposition time was increased. On the one hand, the peak potential shifted to slightly more positive potentials as the deposition potential was made more negative, which also effected a gradual decrease of the Q_{ox}/Q_{red} ratio. On the other hand, for the deposits obtained from the [Sn(II)]/[Co(II)] = 1/2 bath at deposition potentials more negative than −1000 mV, hydrogen evolution was evident, even for short deposition times. In these cases the stripping curves showed nearly no current, in agreement with the voltammetric results at very negative limits. Similar behaviour was observed for [Sn(II)]/[Co(II)] ratios greater than 1/5.

With deposits obtained from solutions with [Sn(II)]/[Co(II)] ratios lower than 1/5, a more positive second stripping peak appeared (peak II), which increased upon decreasing the deposition potential (Figure 4A) and increasing the deposition time (Figure 4B). In all cases peak I appears first, peak II being observed only with deposition times longer than a few seconds. When peak II predominates, a high Q_{ox}/Q_{red} is always obtained.

3.3. *Morphological, compositional and structural results*

Morphological, structural and compositional analysis of the deposits obtained under different experimental conditions were carried out in order to correlate the type of deposit obtained with the electrochemical response. The deposits were effected on a copper substrate in order to improve the adherence. The stripping curves of deposits on copper (Figures 5(a) and 6(a)) were similar to those of deposits on vitreous carbon (Figures 3 and 4), and this was also the case for long deposition times.

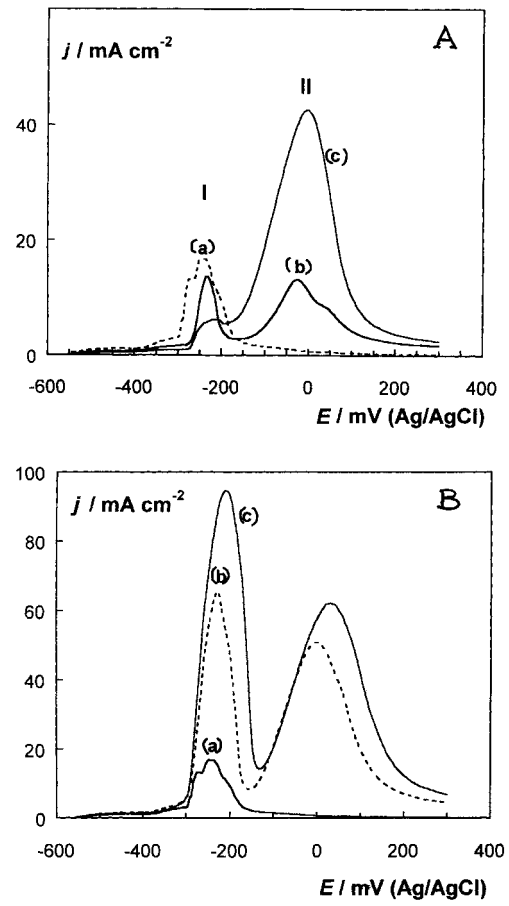

Fig. 4. Stripping voltammograms of deposits obtained potentiostatically on a vitreous carbon electrode rotating at 1000 rpm in a 0.1 M $CoSO_4$ + 0.01 M $SnSO_4$ + 0.2 M $NaC_6H_{11}O_7$ + 0.2 M Na_2SO_4 solution. (A) With a deposition time of 20 s at: −950 mV (curve (a)), −1000 mV (curve (b)) and −1050 mV (curve (c)). (B) Deposition at −950 mV for 20 s (curve (a)), 60 s (curve (b)) and 100 s (curve (c)).

To facilitate the correlation between stripping curves and type of deposit, deposition conditions were chosen such that only one stripping peak appeared. Previously, it was confirmed that, irrespective of the deposition conditions chosen, the potential of the stripping peak did not change much upon increasing the deposit thickness, although, as usually observed, stripping curves are not useful for thicker deposits.

Deposits yielding the stripping peak I were favoured from baths with [Sn(II)]/[Co(II)] ratios greater than 1/5 and for not too negative deposition potentials, near that at which only Sn is deposited. Figure 5(b) and (c) show the morphology of these deposits, obtained from a bath with [Sn(II)]/[Co(II)] = 1/2 at −950 mV. The morphology of the deposit obtained with 5 min of deposition is shown in Figure 5(b). The deposit contained 34% Co by weight, which corresponds to an atomic Sn:Co ratio of 1:1. With longer deposition times a second growth occurred (Figure 5(c)), which corresponded to tin with a very low Co content, less than 0.3%. The deposition time that

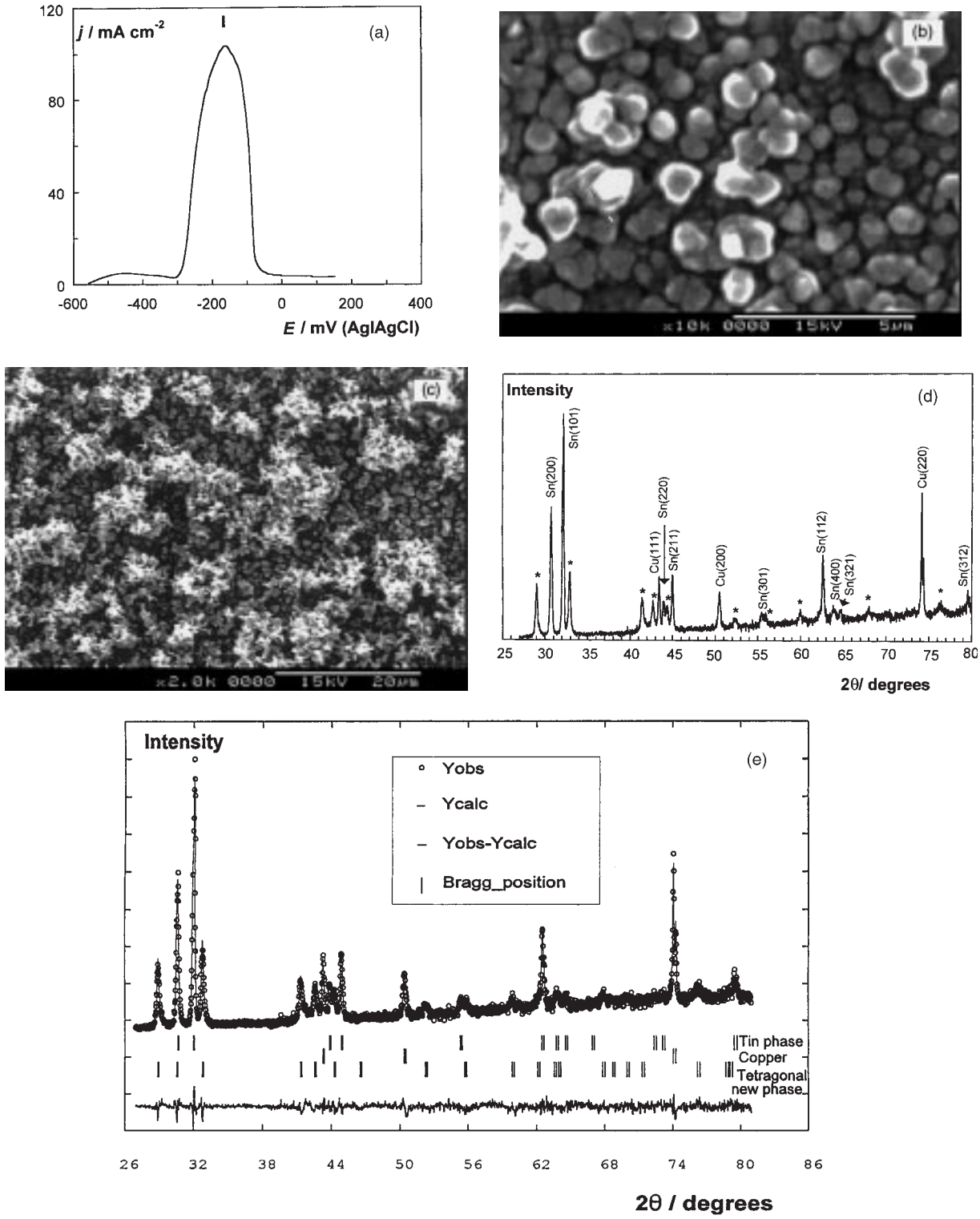

Fig. 5. Deposit obtained on a copper electrode rotating at 1000 rpm in a 0.06 M $CoSO_4$ + 0.03 M $SnSO_4$ + 0.2 M $NaC_6H_{11}O_7$ + 0.2 M Na_2SO_4 solution at a deposition potential of −950 mV. (a) Stripping voltammogram of deposit obtained for 30 s. (b) SEM micrograph of deposit obtained during 5 min. (c) SEM micrograph of deposit obtained during 20 min. (d) X-ray diffractogram of deposit of Figure 5(c). The peaks marked '*' are the main peaks of the new tetragonal SnCo phase, and are listed in Table 1. (e) Profile pattern matching of the diffractogram of Figure 5(d).

gave only the homogeneous phase with a Co content of 34% w/w, and consequently the thickness of this homogeneous deposit, depended on experimental conditions.

The diffractograms of these deposits showed narrow peaks (Figure 5(d)), some of which correspond to very slightly modified tin, and the other ones (labelled '*') do not correspond to any of the phases described in the thermal phase diagram of the tin–cobalt system [14]. All these peaks have been introduced in the TREOR indexation program [15], which assigned them to a

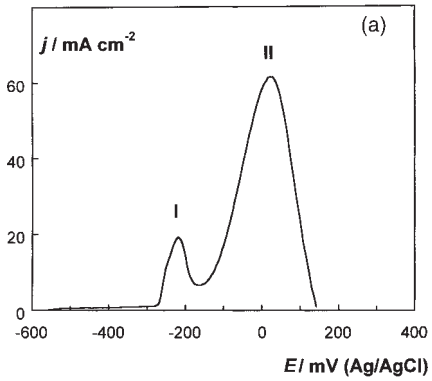

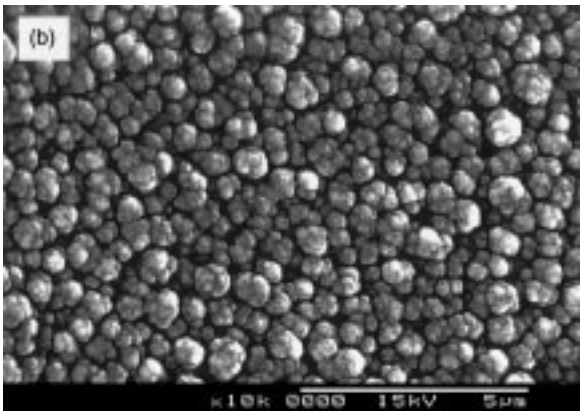

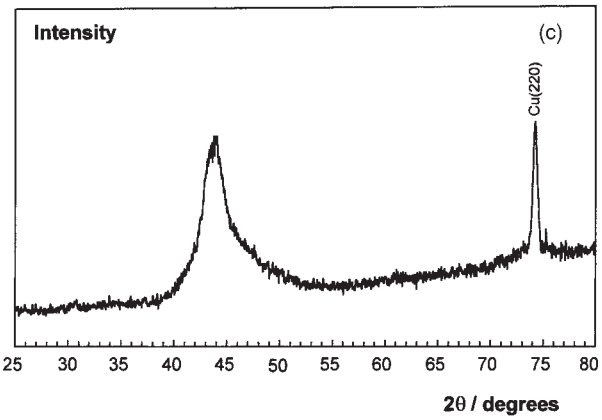

Fig. 6. (a) Stripping voltammogram of deposit obtained with 20 s at −1050 mV on a copper electrode rotating at 1000 rpm in a 0.1 M $CoSO_4$ + 0.01 M $SnSO_4$ + 0.2 M $NaC_6H_{11}O_7$ + 0.2 M Na_2SO_4 solution. (b) SEM micrograph of deposit obtained under the same conditions of Figure 6(a), but with 20 min at −1020 mV. The deposit contained 65% Co w/w. (c) X-ray diffractogram of the Sn + Co deposit of Figure 6(b).

new tetragonal phase. The cell parameters of this tetragonal structure have been refined, together with the tin phase parameters and those corresponding to the copper substrate, by profile pattern matching using FULLPROF [16]. All the peaks of the diffractogram could be indexed (Figure 5(e)). A list of the 2θ positions, $h\ k\ \ell$ indexes and relative intensities of the main peaks is given in Table 1. The cell parameters assigned to the new tetragonal phase are $a = 3.087\ 0(3)$ Å and $c = 5.849\ 0(11)$ Å.

Deposits yielding the stripping peak II were favoured with [Sn(II)]/[Co(II)] ratios lower than 1/5 and for deposition potentials more negative than −1000 mV. Figure 6(b) shows the morphology of deposits yielding mainly peak II. Homogeneous deposits with nodular morphology were obtained in the range of −980 to −1050 mV. These deposits are cobalt rich, in all cases the Co percentage in the deposits increasing when the deposition potential was made more negative.

The diffractogram corresponding to these nodular deposits which yield peak II showed (Figure 6(c)) only one broad, irregular peak around $2\theta = 44°$, next to the (1 1 1) line of cobalt. This deposit appeared to correspond to a single phase with a significant preferred orientation, with a partially amorphous structure, or with a crystalline structure of nanometric crystal size. The latter hypothesis was confirmed by an estimation of the crystallite size domain from the broadening of the peaks, using Scherrer's equation.

Table 1. Main peaks of the new SnCo tetragonal phase

2θ position (CuK_α)/degrees	$h\ k\ \ell$	I/I_o
28.900	1 0 0	0.84
32.777	1 0 1	1
41.328	1 1 0	0.82
42.548	1 0 2	0.66
44.254	1 1 1	0.60
52.252	1 1 2	0.39
55.717	1 0 3	0.58
59.876	2 0 0	0.63
67.831	2 1 0	0.29
76.197	2 1 2	0.31

4. Discussion

Stripping analysis has been revealed as a useful tool for detecting the initial formation of each Sn + Co alloy type, since a direct correlation between the stripping curve and the morphology and structure of the deposits has been found. Two major stripping peaks are observed, each one related to the formation of a kind of deposit. Peak I is related to a new SnCo tetragonal phase, while peak II corresponds to Co-rich nanocrystalline deposits.

The SnCo tetragonal phase is a new phase that does not appear in the thermal phase diagram, [14]. Other tetragonal structures have been proposed for Sn–Co

alloys obtained either thermally or by electrodeposition, but they are different from that reported here. Hemsley et al. [1] and Abd el Rehim et al. [8] proposed the formation of a $CoSn_2$ tetragonal structure from a gluconate bath under different conditions, the latter authors assigning the cell parameters to the thermal $CoSn_2$ phase.

The same 1:1 stoichiometry of our SnCo phase was observed for the Sn + Ni system, for which a metastable SnNi phase can also be obtained either by electrodeposition or sputtering techniques, although for SnNi a hexagonal structure was identified [17, 18].

The SnCo phase oxidizes at potentials corresponding to peak I, which are similar to those of pure Sn oxidation. The SnCo phase is very electrocatalytic for hydrogen evolution, which may be the cause of the suppression of SnCo formation at the low negative potentials. The simultaneous hydrogen evolution produces a local pH increase, even under stirring, that favours the precipitation of hydroxides. This fact provokes the clear diminution of Co(II) in the surroundings of the electrode specially for the higher [Sn(II)]/[Co(II)] ratios. Then, cobalt deposition already unfavoured at these low negative potentials, is slowed still further and, while tin precipitation may still take place, and tin deposition becomes the main process. Also, due to the hydroxide precipitation the peak potential of peak I increases with increasingly negative deposition potentials, that is, with increasing formation of hydroxides.

The SnCo phase is formed at deposition potentials more negative than those at which pure Sn deposition occurs. In all conditions SnCo is the first deposit formed, and is favoured by solutions with higher Sn(II) concentrations, although for the highest one used here the deposition of the more noble metal (Sn) is favoured after some minutes of SnCo electrodeposition. Therefore, with higher [Sn(II)]/[Co(II)] ratios it is necessary to control the electrodeposition charge in order to obtain thin films of tin-rich tetragonal deposits (SnCo). The thickness of the SnCo film depended strongly on the deposition potential as well.

Moreover, working at the lower [Sn(II)]/[Co(II)] ratios, the bath used allowed us to obtain, after deposition of some initial SnCo, coherent Co-rich nanocrystalline deposits. The cobalt contents increased with increasingly negative electrodeposition potential. These deposits oxidize at potentials corresponding to peak II, at more positive values than that corresponding to pure Co, which indicates that the presence of some Sn in the deposit leads to an alloy more noble than pure Co.

Acknowledgements

The authors thank the Serveis Científico-Tècnics (Universitat de Barcelona) for equipment availability. This research was supported financially by contract MAT 97-0379 of the Comisión Interministerial de Ciencia y Tecnología (CICYT) and by the Comissionat of the Generalitat de Catalunya under Research Project SGR98-027.

References

1. J.D.C. Hemsley and M.E. Roper, *Trans. Inst. Met. Fin.* **57** (1979) 77.
2. P.K. Datta, 'Coatings and Surface Treatment for Corrosion and Wear Resistance', (K.N. Strafford, P.K. Datta and G.C. Gookan (Ed.) Chichester: Ellis Horwood, 1984) p. 74.
3. R. Sabitha, Malathy Pushpavanam, M. Mahesh Sugatha and T. Vasudevan, *Trans. Met. Fin. Ass. of India* **5** (1996) 267.
4. M. Degrez and R. Winand, Second Congress on 'Cobalt Metallurgy and Uses', (Cobalt Development Institute, Bruxelles, 1986), p. 432.
5. V.N. Kudryavtsev, K.M. Tyutina, A.N. Popov, S.A. Maksimenko and V.A. Zonin, *Plat. Surf. Finish.* **79** (1992) 57.
6. S. John, N.V. Shanmugan and S. Guruviah, *Metal Finish.* **87** (1989) 19.
7. J.M. Bowden, *Product Finish.* **44** (1991) 6.
8. S.S. Abd Rehim, S.A. Refaey, G. Schwitzgebel, F. Taha and M.B. Saleh, *J. Appl. Electrochem.* **26** (1996) 413.
9. J. Jaén, M.L. Varsanyi, E. Kovács, I. Czakó-Nagy, A. Buzás, A. Vértes and L. Kiss, *Electrochim. Acta* **29** (1984) 119.
10. V.D. Jovic, R.M. Zejnilovic, A.R. Despic, and J.S. Stevanovic, *J. Appl. Electrochem.* **18** (1988) 511.
11. E. Gómez, X. Alcobe and E. Vallés, *J. Electroanal. Chem.* **475** (1999) 66.
12. M.L. Alcalá, E. Gómez and E. Vallés, *J. Electroanal. Chem.* **370** (1994) 73.
13. E. Gómez, J. Ramirez and E. Vallés, *J. Appl. Electrochem.* **28** (1998) 71.
14. H. Baker (Ed), 'ASM Handbook', Vol. 3, 'Alloy Phase Diagrams', (ASM International, Ohio, 1992).
15. P.E. Werner, L. Eriksson and M. Westdah, *J. Appl. Cryst.* **18** (1985).
16. J. Rodriguez-Carvajal, Satellite Meeting on 'Powder Diffraction' of the XV Congress of the IVCr, Tolouse, France (1990), p. 127.
17. J.A. Augis and J.E. Bennett, *J. Electrochem. Soc.* **125** (1978) 335.
18. J.E. Bennett and H.G. Tomphus, *J. Electrochem. Soc.* **123** (1976) 999 and references therein.